

High-temperature-grown buffer layer boosts electron mobility in epitaxial La-doped BaSnO₃/SrZrO₃ heterostructures

Arnaud P. Nono Tchiomo,^{1,2} Wolfgang Braun,¹ Bryan P. Doyle,² Wilfried Sigle,¹ Peter van Aken,¹ Jochen Mannhart,¹ and Prosper Ngabonziza^{1,2, a)}

¹⁾Max Planck Institute for Solid State Research, Heisenbergstr. 1, 70569 Stuttgart, Germany

²⁾Department of Physics, University of Johannesburg, P.O. Box 524 Auckland Park 2006, Johannesburg, South Africa

(Dated: 1 April 2019)

By inserting a SrZrO₃ buffer layer between the film and the substrate, we demonstrate a significant reduction of the threading dislocation density with an associated improvement of the electron mobility in La:BaSnO₃ films. A room temperature mobility of 140 cm² V⁻¹s⁻¹ is achieved for 25-nm-thick films without any post-growth treatment. The density of threading dislocations is only 4.9 × 10⁹ cm⁻² for buffered films prepared on (110) TbScO₃ substrates by pulsed laser deposition.

Transparent conducting oxides (TCOs) have attracted attention due to their unique properties and applications in electronic devices such as transparent displays and transistors.^{1,2} Recently, the transparent perovskite La:BaSnO₃ has gained interest as a novel TCO due to its high mobility at room temperature (RT).^{3,4} Single crystals of La:BaSnO₃ have been reported to have RT mobilities as high as 320 cm² V⁻¹s⁻¹ (mobile carrier concentration $n = 8 \times 10^{19}$ cm⁻³).⁴ At doping concentrations above 10¹⁹ cm⁻³, La:BaSnO₃ has the second highest RT electron mobility among TCOs and other oxide single crystals⁴⁻⁶, exceeded only by CdO.⁷ The high RT mobility in La:BaSnO₃ has been attributed to the small electron-phonon interaction and small electron effective mass ($m_e^* = 0.19 m_0$) arising from the large dispersion of the conduction band comprised of Sn 5s orbitals.⁸⁻¹⁰ However, to fully explore the potential of La:BaSnO₃, thin films with high mobilities are also required.

Recently, several efforts to achieve high carrier mobility in La:BaSnO₃ films have been reported.¹¹⁻¹⁸ Nevertheless, as compared to bulk single crystals, even the best La:BaSnO₃ epitaxial films show a reduced mobility (≤ 183 cm² V⁻¹s⁻¹),¹⁸ which specifically has been attributed to scattering from charge defects, such as threading dislocations (TDs)^{8,18-20} and, more generally, to small carrier relaxation times.^{8,9} TDs form for a large lattice mismatch between film and substrate, and extend perpendicularly through the films. The obvious solution to reduce TDs in La:BaSnO₃ films is to use lattice-matched substrates, but unfortunately none exists. The substrate with the closest lattice match that is commercially available is PrScO₃, mismatched by -2.3%.²¹ With such a high mismatch only thin commensurate layers of BaSnO₃ can be grown; at a thickness of 32 nm the reported BaSnO₃ films are almost fully relaxed and contain high densities of TDs.¹⁹

To reduce the dislocation density in the La:BaSnO₃ film, we explored the insertion of an undoped BaSnO₃

buffer layer at the interface between the substrate (TbScO₃) and the La:BaSnO₃ film. As the thickness of the BaSnO₃ layer increases, the TD density decreases as the threading component of dislocations annihilate each other, leaving behind a network of misfit dislocations. This method is known and has already led to the highest mobilities in BaSnO₃ films to date; but even for thick buffer layers (330 nm), the remaining TD density is still 1.2 × 10¹¹ cm⁻².¹⁸ Conceptually, growing this undoped BaSnO₃ buffer layer at higher substrate temperatures should lower TD densities further, but due to the significant volatility of tin oxide at substrate temperatures above about 850°C, this is not a viable option.

In this work, we report on an alternative approach to significantly reduce the dislocation density and increase the mobility of La:BaSnO₃ films. By inserting between the film and the substrate an insulating buffer layer of SrZrO₃ grown at very high temperature, we greatly reduce the density of TDs. To avoid possible contamination, we first optimized the growth conditions of the films on (110) TbScO₃ substrates thermally prepared *in situ* by directly heating the substrate with a CO₂ laser. Without resorting to post-growth treatments, we achieve a significant reduction of the density of TDs from 5 × 10¹¹ cm⁻² to 4.9 × 10⁹ cm⁻² and a maximum RT mobility of 140 cm² V⁻¹s⁻¹ for La:BaSnO₃ films prepared on a SrZrO₃ buffer (grown at 1300 °C). Extending prior reports, this RT mobility is obtained for films of small thickness (25 nm). It is the highest mobility for La:BaSnO₃ films grown by PLD.

Epitaxial La:BaSnO₃ films with a La-doping content of 6% and a thickness of 25 nm were grown on several (110) oriented TbScO₃ single crystalline substrates (5 × 5 × 1 mm³). All samples were grown by PLD ($\lambda = 248$ nm) at a target-substrate distance of 56 mm, using a CO₂ laser substrate heating system. The La:BaSnO₃ films were grown at 850 °C and 1.5 J cm⁻² at 1 Hz in 1 × 10⁻¹ mbar of O₂. Films were grown on either SrZrO₃ or BaSnO₃ buffer layers. The buffer layers were deposited at 4 Hz to a thickness of 100 nm. We chose SrZrO₃ as a candidate because its lattice parameter value (4.101 Å)^{22,23} is be-

^{a)}Corresponding author: p.ngabonziza@fkf.mpg.de

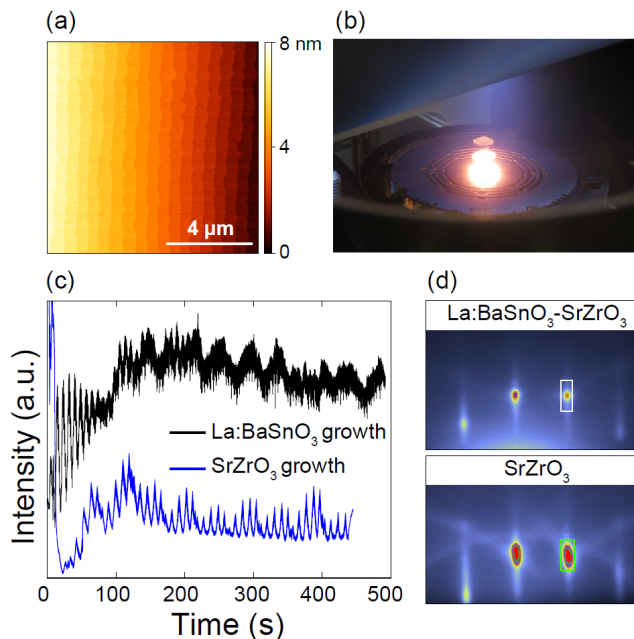


FIG. 1. (a) AFM image of a typical (110) TbScO_3 substrate annealed *in situ* at 1300 °C for 200 sec. (b) Inside view image of the PLD chamber showing a TbScO_3 substrate at 1600 °C with a plume ejected from the SrZrO_3 target during PLD growth. Due to multiple reflections, several images of the hot substrate are superimposed. (c) Reflection high-energy electron diffraction (RHEED) intensity oscillations during the growth of a SrZrO_3 buffer layer at 1300 °C (blue) and La:BaSnO_3 film at 850 °C (black). (d) RHEED patterns viewed along the [110] azimuth of (top) a 25 nm thick La:BaSnO_3 film grown on top of (bottom) a 100 nm thick SrZrO_3 buffer layer. The green and white rectangles mark the region from which the integrated intensity as a function of time during deposition in (c) were recorded.

tween that of La:BaSnO_3 (4.116 Å) and TbScO_3 (3.955 Å).²⁴ Also, like TbScO_3 , SrZrO_3 has a low vapor pressure and can therefore be grown at high temperatures. SrZrO_3 layers were deposited at temperatures ranging from 850 °C to 1600 °C with a laser fluence of 2 J cm^{-2} at 1.4×10^{-2} mbar of O_2 . The BaSnO_3 buffer layers were grown at 850 °C with a fluence of 1.5 J cm^{-2} at 1×10^{-1} mbar of O_2 . Following Ref.¹⁸, BaSnO_3 was chosen as it has roughly the same lattice parameter as La:BaSnO_3 .

Prior to deposition, the TbScO_3 substrates were *in situ* terminated at high temperature with the CO_2 laser. Figure 1(a) shows a typical atomic force microscopy (AFM) image of thermally prepared substrates heated at 1300 °C for 200 s. The substrate surface is smooth and well-ordered, with clear and uniform terraces. More details on the *in situ* thermal preparation of the substrates and related oxide surfaces are provided in Ref. 25. Figure 1(b) shows a photograph of the growth chamber during the deposition of the SrZrO_3 buffer layer at 1600 °C.

The deposition of both the active layer (La:BaSnO_3) and buffer layer (SrZrO_3) were *in situ* monitored by reflection high-energy electron diffraction (RHEED)

[Fig. 1(c)]. The SrZrO_3 layer was deposited at 1300 °C. Immediately after the deposition, the sample was cooled to 850 °C at 2 K/sec for the subsequent growth of the La:BaSnO_3 film. We observe that the intensity of the RHEED oscillations remains the same throughout the deposition of the SrZrO_3 layer. For the La:BaSnO_3 film, the intensity drops after several monolayers and then stabilizes. The intensity drop suggests a relaxation in the film after a critical thickness has been reached (see Fig. S1 of the supplementary material). The RHEED data indicate that the SrZrO_3 buffer layer and the La:BaSnO_3 films are grown in a layer-by-layer mode with a smooth surface as also demonstrated by streaky RHEED patterns for both layers [see Fig. 1(d)].

The crystalline quality and phase purity of the films were characterized by X-ray diffraction (XRD) using $\text{Cu K}\alpha$ radiation. Figure 2(a) shows the $2\theta - \omega$ scans around the 002 diffraction planes for the $\text{La:BaSnO}_3/\text{TbScO}_3$ (sample A1), $\text{La:BaSnO}_3/\text{BaSnO}_3/\text{TbScO}_3$ (sample A2) and $\text{La:BaSnO}_3/\text{SrZrO}_3/\text{TbScO}_3$ (sample A3) films. Laue thickness fringes and phase-pure La:BaSnO_3 00l peaks are observed, indicating smooth growth and high crystallinity [Fig. 2(a), see also Fig. S2 of the supplementary material]. The film thicknesses were extracted from the Laue thickness fringes and the Kossel fringes observed by XRD. The extracted out-of-plane lattice parameters are $c = 4.134$ Å, 4.120 Å and 4.113 Å for samples A1, A2 and A3. These values are consistent with the out-of-plane lattice constants reported previously for La:BaSnO_3 films^{20,26} and are close to the bulk lattice parameter (~ 4.126 Å) of polycrystalline 6% La:BaSnO_3 .^{27,28} Figures 2(b) and 2(c) show reciprocal space maps (RSM) around the asymmetric $(\bar{1}03)_p$ reflection peaks of the films (samples A2 and A3) and the substrate. The in-plane and out-of-plane lattice constants of the film in sample A2 are $a = 4.117$ Å and $c = 4.120$ Å, respectively, indicating that the film is almost completely relaxed. The relatively small deviation of the lattice constants is attributed to the large lattice mismatch (3.9%) between BaSnO_3 and the TbScO_3 [Fig. 2(b)]. The broadening of the film peak indicates the presence of a large density of dislocations. For sample A3, the extracted in-plane and out-of-plane lattice constants are $a = 4.103$ Å, $c = 4.113$ Å, indicating that the film is fully strained in the a direction (-0.56%) and partially relaxed in the c direction. From the XRD data (see Fig. S3 of the supplementary material) of a control sample of SrZrO_3 grown at 1300 °C (in the same growth conditions as the buffer layer in sample A3), in-plane and out-of-plane lattice constants of $a = 4.085$ Å and $c = 4.128$ Å are obtained, indicating that the buffer layer is almost fully strained to the substrate (3.966 Å), suggesting a small number of dislocations in the film A3 as discussed below.

Resistivity (ρ), electron mobility (μ_e) and carrier concentration (n) were characterized in a physical property measurement system (PPMS) in a van der Pauw geometry by wire bonding aluminum wires to the samples' corners. An excitation current of 1 μA was used. Using the

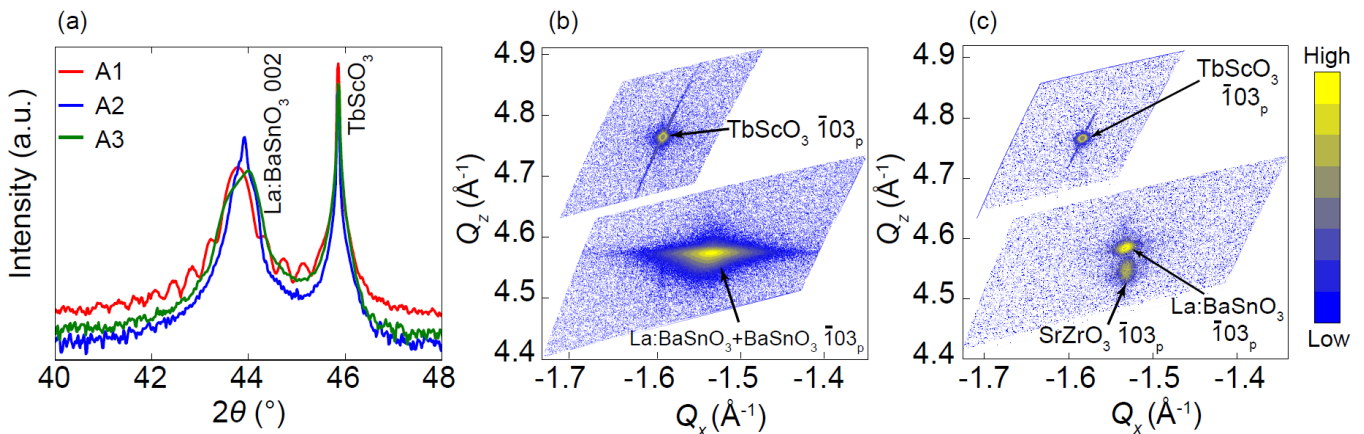


FIG. 2. XRD scans of 25 nm thick La:BaSnO₃ films. (a) A close-up view of the $2\theta-\omega$ scan around the 002 peak for La:BaSnO₃ film grown directly on (110) TbScO₃ (red curve), and La:BaSnO₃ films deposited on top of BaSnO₃ (blue curve) and SrZrO₃ (green curve) buffer layers grown on (110) TbScO₃. The 002 peaks of La:BaSnO₃ show thickness fringes. Reciprocal space maps of samples A2 and A3 in (a) around the $\bar{1}03_p$ reflection peaks of the (b) La:BaSnO₃/BaSnO₃ and (c) La:BaSnO₃/SrZrO₃ heterostructures, and the $\bar{1}03_p$ reflection of TbScO₃ substrates, where p refers to pseudo-cubic indices.

procedure discussed in Refs.^{29,30}, the carrier concentration was calculated as $n = 1/eR_H$, where R_H is the measured Hall coefficient; and the electron mobility was extracted from $\mu_e = R_H/\rho$, where ρ was determined by the Van der Pauw method. Figure 3(a) presents the temperature dependence of the resistivity at zero magnetic field for the samples A1, A2 and A3. All films exhibit metallic behavior over the entire temperature range, consistent with previous reports on La:BaSnO₃.^{3,4} The temperature dependence of the carrier density shows the behavior of a degenerate semiconductor.³ The concentration of the negatively charged carriers is temperature independent at high temperatures, but starts to decrease below 50 K following the freeze out at the La⁺³ ions [Fig. 3(b)].³¹ The temperature dependence of the electron mobility is presented in Fig. 3(c). For all three samples, μ_e increases down to the lowest temperature (2 K), contrary to previous studies which reported a saturation below 50 K.^{18,19} This behavior suggests a significant reduction of phonon scattering for these films at low temperatures. For the sample directly grown on the substrate (A1), a mobility of $76 \text{ cm}^2 \text{ V}^{-1}\text{s}^{-1}$ (RT) was measured. In the sample with the BaSnO₃ buffer layer (A2), the RT μ_e is improved to $117 \text{ cm}^2 \text{ V}^{-1}\text{s}^{-1}$, but apparently still limited by the high density of TDs, as discussed below. To reduce the density of TDs, we switched to SrZrO₃ buffer layers. Several La:BaSnO₃/SrZrO₃ heterostructures were prepared by varying the growth temperatures of the SrZrO₃ layer from 850 °C to 1600 °C, while keeping the other growth parameters constant. We find 1300 °C as the optimal growth temperature of the SrZrO₃ buffer layer to achieve high mobility in the La:BaSnO₃ layers [Fig. 3(d)]. Above 1300 °C the buffer layers start to become more non-stoichiometric, i.e., the ratio of Sr:Zr deviating from 1 in SrZrO₃ due to the volatility of constituents³ (see Fig. S3(d) in supplemental materials). This results in an enhanced defect density (e.g. shear defects and/or

point defects arising from nonstoichiometry¹⁸), limiting the mobility of the La:BaSnO₃ layers deposited on buffer layers grown at temperatures above 1300 °C. The sample A3 prepared on a buffer layer grown at 1300 °C has the highest mobility $\mu_e = 140 \text{ cm}^2 \text{ V}^{-1}\text{s}^{-1}$ (RT) and $375 \text{ cm}^2 \text{ V}^{-1}\text{s}^{-1}$ (2 K) [Fig. 3(c)]. For PLD grown La:BaSnO₃ thin films, this RT μ_e is $\sim 30\%$ higher than the previous record ($100 \text{ cm}^2 \text{ V}^{-1}\text{s}^{-1}$) achieved without post-growth treatment on BaSnO₃ substrates;²⁶ and

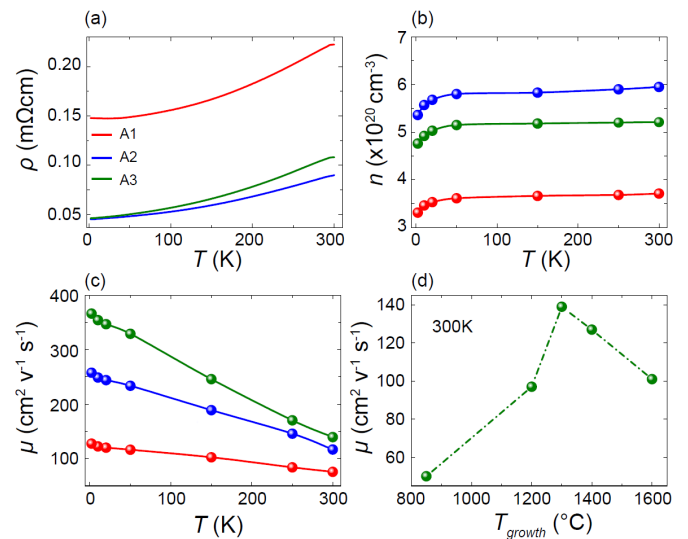


FIG. 3. Transport characteristics of 25 nm La:BaSnO₃ films. (a) Temperature dependence of the zero-field resistivity of the samples (red) A1, (blue) A2 and (green) A3. (b) Mobile electron carrier concentration vs. temperature and (c) electron mobility vs. temperature of the same La:BaSnO₃ films characterized in Figs. 1(c)-(d) and Fig. 2. (d) Measured electron mobility as function of the growth temperature of the SrZrO₃ buffer layer.

15% higher than reported enhanced mobility ($122 \text{ cm}^2 \text{ V}^{-1} \text{ s}^{-1}$) after post-annealing processes in H_2 forming gas at $950 \text{ }^\circ\text{C}$ on SrTiO_3 .³³

To further investigate the role of TDs that act as scattering centers and trap electrons,^{8,13,20,34} we studied the defect structure of the samples A2 and A3 using cross-sectional transmission electron microscopy (TEM). Figures 4(a) and 4(b) present the weak-beam dark-field TEM (WB-DFTEM) images of the entire film thickness for the samples A2 and A3, respectively. For both samples misfit dislocations are visible along the interface as bright dots, indicated in figures 4(a) and 4(b) by red arrows. To accommodate the large lattice mismatch between the substrate and the film, these misfit dislocations generate edge-type defects, which extend vertically through the film (bright contrast indicated by white arrows in Fig. 4(a)). For a TEM specimen of 16 nm thick, the extracted density of TDs in sample A2 was $5 \times 10^{11} \text{ cm}^{-2}$. This density of TDs is in agreement with previous reports on La:BaSnO_3 films prepared on DyScO_3 ¹⁸ and SrTiO_3 ²⁰ substrates. Interestingly, TDs were barely observed in the highest mobility sample A3 as shown in the WB-DFTEM image in Fig. 4(b). Even for a TEM specimen of 205.5 nm thick, the TDs density was $4.9 \times 10^9 \text{ cm}^{-2}$ which is two orders of magnitude lower than the one in the sample A2 and previously reported TD densities for La:BaSnO_3 films.^{18,20} Figures 4(c) and 4(d) depict the high resolution TEM images of samples A2 and A3, respectively. A fully relaxed interface between the TbScO_3 substrate and the BaSnO_3 layer is seen in sample A2 as indicated by white circles. Additional structural defects such as stacking faults are also visible in the film [see yellow arrows in Fig. 4(c)]. On the other hand, a strained interface is seen in sample A3 with no apparent structural defects [Fig. 4(d)].

The low density of TDs in sample A3 is attributed to the high temperature used for the SrZrO_3 buffer layer growth. One of the effective ways of minimizing the TDs density is to enhance the motion and reaction of TDs by high thermal stress. This method was demonstrated to be efficient in epitaxial semiconductor GaAs films on Si substrates.^{35,36} At high temperatures, the velocity of the dislocations glide motion and the concentration of vacancies that support the climb motion of the dislocations are exponentially enhanced.³⁷ Thus, the observed significant reduction of the TDs density in sample A3 is attributed to the enhancement of the glide and climb motion at high temperatures. Stress that increases the glide motion originates from the difference in the thermal expansion coefficients of ~ 3.1 between SrZrO_3 and TbScO_3 ^{38,39} and also possible grown-in strain in the SrZrO_3 layer. The latter is supported by the fact that SrZrO_3 undergoes a phase transition from tetragonal to cubic at high temperature,³⁹ indicating epitaxial strain at the interface during cool down, yielding a reduction of the lattice mismatch. Our results suggest that the high temperature grown SrZrO_3 epilayer deposited not only on TbScO_3 but also on other oxide substrates (e.g. SrTiO_3 , DyScO_3 ,

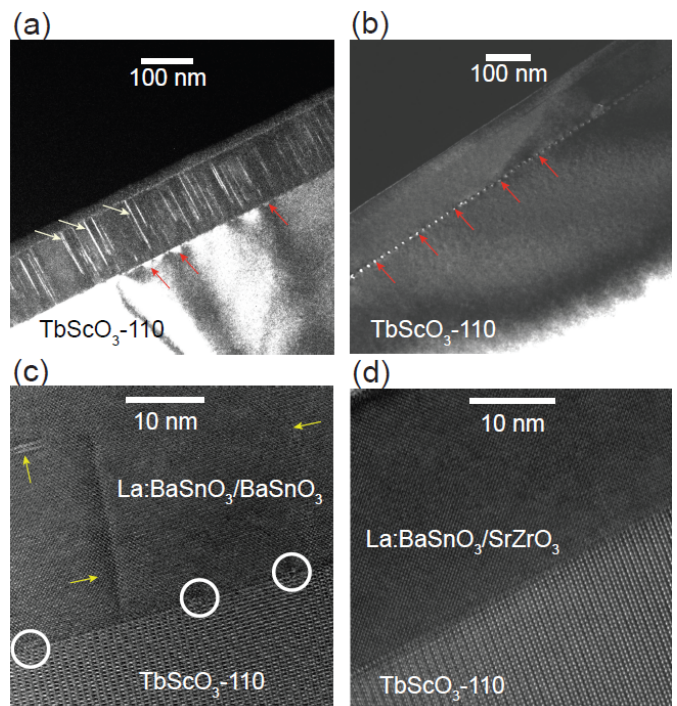


FIG. 4. Weak-beam dark-field TEM images of samples (a) A2 and (b) A3. Misfit dislocations along the interfaces are shown by red arrows. Edge-type threading dislocations are visible in (a), indicated by vertical bright contrasts (white arrows). Only periodic misfit dislocations are visible in (b). Their average distance is 17 nm. High-resolution TEM images for the same heterostructures (c) A2 and (d) A3. Misfit dislocations indicated by white circles in (c) suggest a fully relaxed interface. Stacking faults (yellow arrows) are also visible. An almost fully strained interface is seen in (d) with no apparent structural defects.

MgO) can be utilized as a template for subsequent growth of high mobility La:BaSnO_3 films with fewer TDs.

Although we have demonstrated that by inserting a high-temperature grown SrZrO_3 buffer layer between the film and the substrate the density of TDs significantly reduces with an associated improvement of the electron mobility in La:BaSnO_3 films, we point to several observations. Normally, scattering by TDs not only diminishes the electron mobility, but also reduces the number of free charge carriers²⁰. However, we observe that the carrier density of sample A2 (with the high density of TDs) is higher than sample A3 (with a low TD density) [Fig. 3(b)]. Given that the active layer in our samples is thin (25 nm), the lower number of free charge carriers in sample A3 suggests that not only TDs are trapping electrons, but that also effects such as surface scattering or interface traps are lowering the density of mobile carriers. For the sample A2, these contributions are expected to be less pronounced as the buffer layer (BaSnO_3) and the active layer consist of the same materials.

In summary, we explore the possible use of buffer layers grown at very high temperatures for the reduction

of TDs and improvement of electron mobility in epitaxial La-doped BaSnO₃/SrZrO₃ heterostructures grown on (110) TbScO₃ substrates. For La:BaSnO₃ films prepared on a SrZrO₃ buffer layer grown at 1300 °C a RT mobility of 140 cm² V⁻¹s⁻¹ has been achieved, together with a reduction of the density of TDs to 4.9×10^9 cm⁻², all without post-growth sample treatment. With the insertion of a high temperature grown buffer layer between the La:BaSnO₃ film and the TbScO₃ substrate, the mobility has been doubled, which opens a new road towards high mobilities in La:BaSnO₃ based electronic devices.

We acknowledge valuable discussions with Darrell G. Schlom and Hans Boschker, and thank Helga Hoier and Marion Hagel for technical assistance.

- ¹H. Ohta, K. Nomura, H. Hiramatsu, K. Ueda, T. Kamiya, M. Hirano, H. Hosono, *Solid State Electron.* **47**, 2261 (2003).
- ²W.-J. Lee, H. J. Kim, J. Kang, D. H. Jang, T. H. Kim, J. H. Lee, and K. H. Kim, *Annu. Rev. Mater. Res.* **47**, 391 (2017) and references therein.
- ³H. J. Kim, U. Kim, T. H. Kim, J. Kim, H. M. Kim, B-G. Jeon, W-J. Lee, H. S. Mun, K. T. Hong, J. Yu, K. Char, and K. H. Kim, *Phys. Rev. B* **86**, 165205 (2012).
- ⁴H. J. Kim, U. Kim, H. M. Kim, T. H. Kim, H. S. Mun, B-G. Jeon, K. T. Hong, W-J. Lee, C. Ju, K. H. Kim, and K. Char, *Appl. Phys. Express.* **5**, 061102 (2012).
- ⁵X. Luo, Y. S. Oh, A. Sirenko, P. Gao, T. A. Tyson, K. Char, and S. W. Cheong, *Appl. Phys. Lett.* **100**, 172112 (2012).
- ⁶H. M. I. Jaim, S. Lee, X. H. Zhang, and I. Takeuchi, *Appl. Phys. Lett.* **111**, 172102 (2017).
- ⁷E. Sacht, C. T. Shelton, J. S. Harris, B. E. Gaddy, D. L. Irving, S. Curtarolo, B. F. Donovan, P. E. Hopkins, P. A. Sharma, A. L. Sharma, et al., *Nat. Mater.* **14**, 414 (2015).
- ⁸A. Prakash, P. Xu, A. Faghaninia, S. Shukla, J. W. Ager, C. S. Lo and B. Jalan, *Nat. Commun.* **8**, 15167 (2017).
- ⁹K. Krishnaswamy, B. Himmetoglu, Y. Kang, A. Janotti, and C. G. Van de Walle, *Phys. Rev. B* **95**, 205202 (2017).
- ¹⁰C. A. Niedermeier, S. Rhode, K. Ide, H. Hiramatsu, H. Hosono, T. Kamiya, and M. A. Moram, *Phys. Rev. B* **95**, 161202(R) (2017).
- ¹¹J. Yue, A. Prakash, M. C. Robbins, S. J. Koester, and B. Jalan, *ACS Appl. Mater. Interfaces* **10**, 21061 (2018).
- ¹²K. Fujiwara, K. Nishihara, J. Shiogai, and A. Tsukazaki, *Appl. Phys. Lett.* **110**, 203503 (2017).
- ¹³J. Shin, Y. M. Kim, Y. Kim, C. Park, and K. Char, *Appl. Phys. Lett.* **109**, 262102 (2016).
- ¹⁴C. Park, U. Kim, C. Jong Ju, J. S. Park, Y. M. Kim, and K. Char, *Appl. Phys. Lett.* **105**, 203503 (2014).
- ¹⁵U. Kim, C. Park, T. Ha, Y. M. Kim, N. Kim, C. Ju, J. Park, J. Yu, J. H. Kim, and K. Char, *APL Mater.* **3**, 036101 (2015).
- ¹⁶S. Arezoomandan, A. Prakash, A. Chanana, J. Yue, J. Mao, S. Blair, A. Nahata, B. Jalan, and B. Sensale-Rodriguez, *Sci. Rep.* **8**, 3577 (2018).
- ¹⁷Z. Wang, H. Paik, Z. Chen, D. A. Muller, and D. G. Schlom, *APL Mater.* **7**, 022520 (2019).
- ¹⁸H. Paik, Z. Chen, E. Lochocki, A. Seidner H, A. Verma, N. Tanen, J. Park, M. Uchida, S. Shang, B.-C. Zhou, M. Brützmam, R. Uecker, Z.-K. Liu, D. Jena, K. M. Shen, D. A. Muller, and D. G. Schlom, *APL Mater.* **5**, 116107 (2017).
- ¹⁹S. Raghavana, T. Schumanna, H. Kim, J. Y. Zhang, T. A. Cain, and S. Stemmer, *APL Mater.* **4**, 016106 (2016).
- ²⁰H. Mun, U. Kim, H. M. Kim, C. Park, T. H. Kim, H. J. Kim, K. H. Kim, and K. Char, *Appl. Phys. Lett.* **102**, 252105 (2013).
- ²¹T. M. Gesing, R. Uecker, and J. C. Buhl, *Kristallogr. NCS* **224**, 365 (2009).
- ²²E. Mete, R. Shaltaf, and Ş. Ellialtıođlu, *Phys. Rev. B* **68**, 035119 (2003).
- ²³A. J. Smith and A. J. E. Welch, *Acta Crystallogr.* **13**, 653 (1960).
- ²⁴W. Ma, X. Li, X. Meng, Y. Xue, Y. Bai, W. Chen, and H. Dong, *J. Therm. Spray Tech.* **27**, 1056 (2018).
- ²⁵M. Jäger, G. Laskin, P. Ngabonziza, W. Voesch, P. Wittlich, J. Mannhart, and W. Braun, *In situ thermal preparation of oxide surfaces* (in preparation, 2019).
- ²⁶W. J. Lee, H. J. Kim, E. Sohn, T. H. Kim, J. Y. Park, W. Park, H. Jeong, T. Lee, J. H. Kim, K. Y. Choi, and K. H. Kim, *Appl. Phys. Lett.* **108**, 082105 (2016).
- ²⁷T. Huang, T. Nakamura, M. Itoh, Y. Inaguma, and O. Ishiyama, *J. Mater. Sci.* **30**, 1556 (1995).
- ²⁸C. A. Niedermeier, S. Rhode, S. Fearn, K. Ide, M. A. Moram, H. Hiramatsu, H. Hosono, and T. Kamiya, *Appl. Phys. Lett.* **108**, 172101 (2016).
- ²⁹P. Ngabonziza, M. P. Stehno, H. Myoren, V. A. Neumann, G. Koster, and A. Brinkman, *Adv. Electron. Mater.* **2**, 1600157 (2016).
- ³⁰P. Ngabonziza, Y. Wang, and A. Brinkman, *Phys. Rev. Mater.* **2**, 044204 (2018).
- ³¹P. V. Wadekar, J. Alaria, M. O'Sullivan, N. L. O. Flack, T. D. Manning, L. J. Phillips, K. Durose, O. Lozano, S. Lucas, J. B. Claridge, and M. J. Rosseinsky, *Appl. Phys. Lett.* **105**, 052104 (2014).
- ³²Roman Engel-Herbert, *Molecular beam epitaxy of complex oxides (Book chapter in Molecular Beam Epitaxy)*, edited by Mohamed Henini, Elsevier, Amsterdam, Pages: 417-449 (2013).
- ³³D. Yoon, S. Yu, and J. Son, *NPG Asia Mater.* **10**, 363 (2018).
- ³⁴S. Yu, D. Yoon, and J. Son, *Appl. Phys. Lett.* **108**, 262101 (2016).
- ³⁵D. Deppe, N. Holonyak Jr, K. Hsieh, D. Nam, W. Plano, R. Matyi, and H. Shichijo, *Appl. Phys. Lett.* **52**, 1812 (1988).
- ³⁶Y. Takagi, H. Yonezu, Y. Hachiya, and K. Pak, *Jpn. J. Appl. Phys.* **33**, 3368 (1994).
- ³⁷I. Yonenaga and K. Sumino, *J. Appl. Phys.* **62**, 1212 (1987).
- ³⁸R. Uecker, B. Velickov, D. Klimm, R. Bertram, M. Bernhagen, M. Rabe, M. Albrecht, R. Fornari, and D. Schlom, *J. Cryst. Growth* **310**, 2649 (2008).
- ³⁹D. de Ligny and P. Richet, *Phys. Rev. B* **53**, 3013 (1996).

Supplementary information:

High-temperature-grown buffer layer boosts electron mobility in epitaxial La-doped BaSnO₃/SrZrO₃ heterostructures

Arnaud P. Nono Tchiomo^{1,2}, Wolfgang Braun¹, Bryan P. Doyle², Wilfried Sigle¹, Peter van Aken¹, Jochen Mannhart¹, and Prosper Ngabonziza^{1,2}

¹*Max Planck Institute for Solid State Research, Heisenbergstr. 1, 70569 Stuttgart, Germany*

²*Department of Physics, University of Johannesburg, P.O. Box 524 Auckland Park 2006, Johannesburg, South Africa*

Analysis of RHEED intensity oscillations

Reflection high-energy electron diffraction (RHEED) data were acquired using the Safire data acquisition software. The RHEED gun was a differentially pumped Staib system operated at 30 keV. To fit the RHEED raw data from our samples, we followed the procedure for the analysis of the RHEED intensity oscillations presented in Refs. ^{1,2}. We show below RHEED data of the La:BaSnO₃ active layer and SrZrO₃ buffer layer for the highest mobility sample A3 discussed in the main text.

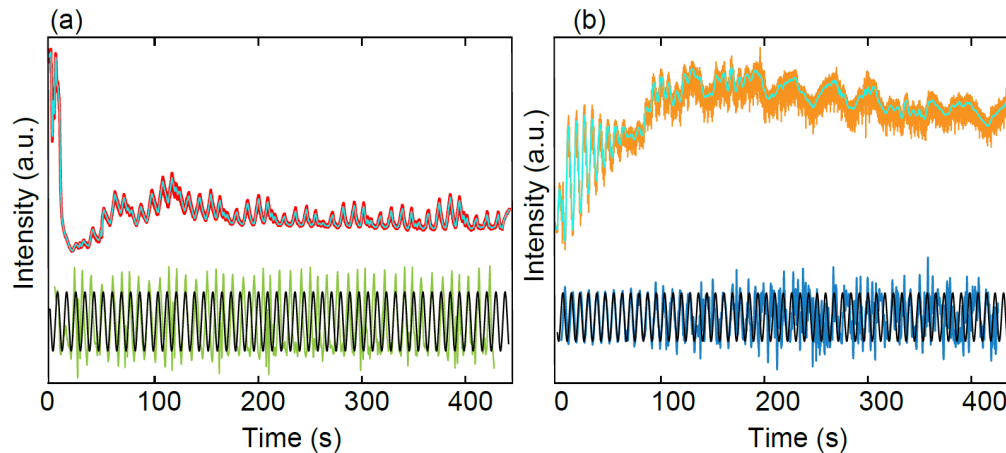


Figure S1: RHEED intensity oscillations during the growth of the sample A3 discussed in the main text. (a) Intensity oscillations during the growth of SrZrO₃ buffer layer (red curve) together with a best fit to the raw data (cyan curve). The bottom green curve was obtained by using an algorithm for RHEED data analysis from Ref. [1] and the transformed data were then fitted by a sine function (black curve). (b) The same analysis was performed on the 25-nm-thick La:BaSnO₃ grown on top of the SrZrO₃ buffer layer.

X-ray diffraction measurements

We present here additional x-ray diffraction (XRD) measurements over a wider region for the samples A1 (La:BaSnO₃/TbScO₃), A2 (La:BaSnO₃/BaSnO₃/TbScO₃) with the buffer layer grown at 850 °C and A3 (La:BaSnO₃/SrZrO₃/TbScO₃) with the buffer layer grown at 1300 °C. Data from these samples are discussed in the main text. Only phase-pure 00*l* peaks from the film are observed, underlining the crystalline quality of the samples.

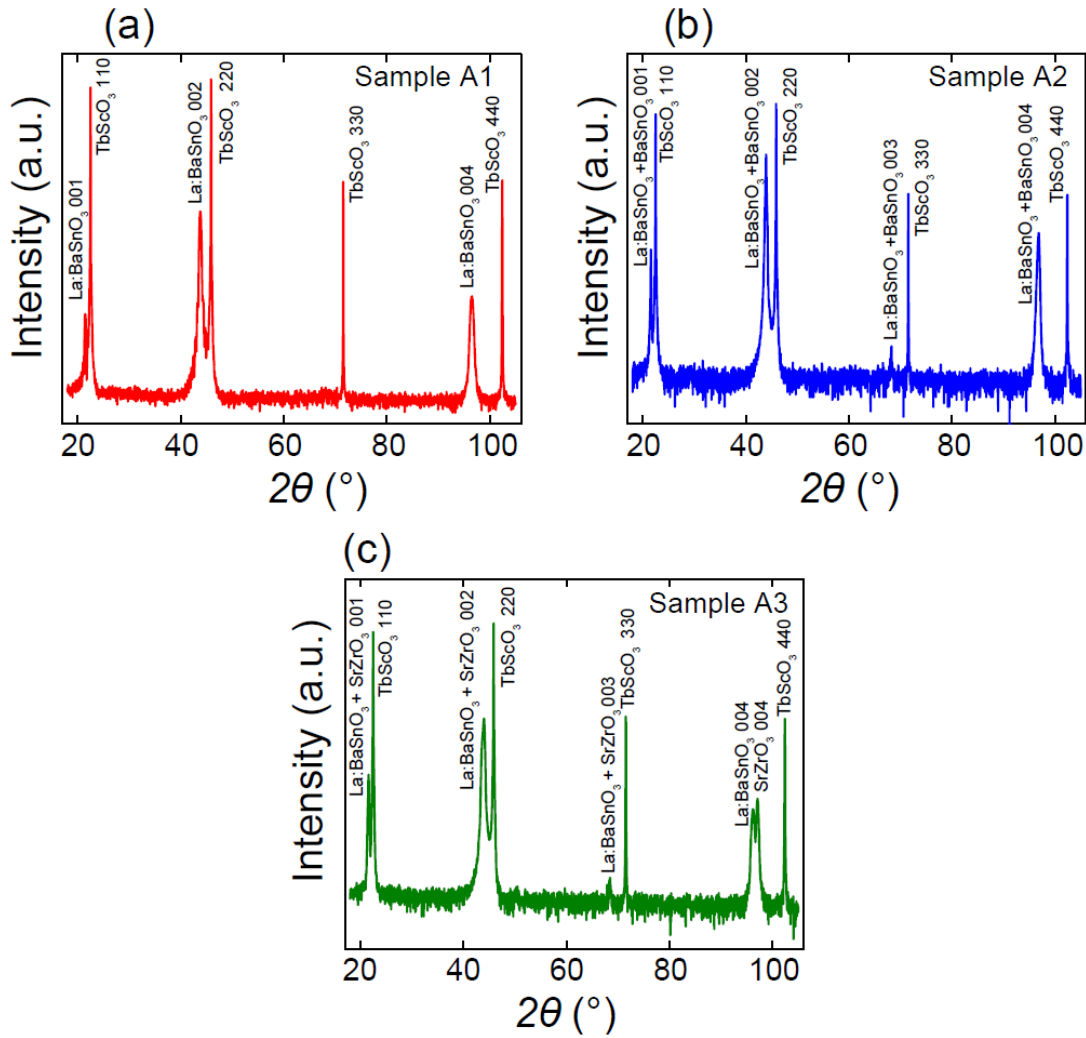


Figure S2: XRD measurements. $2\theta - \omega$ scans over a wider region for the samples (a) A1, (b) A2 and (c) A3 showing only phase-pure $00l$ peaks from the samples.

Characterization of SrZrO_3 buffer layer

XRD and atomic force microscopy (AFM) data for a control sample of SrZrO_3 grown at 1300°C are presented. The sample was prepared in the same growth conditions as the buffer layer in the sample A3 discussed in the main text. The lattice mismatch between SrZrO_3 and TbScO_3 from this control sample grown at 1300°C was reduced from $\sim 3.7\%$ to $\sim 3\%$. As suggested by the SrO partial pressure vs. temperature diagram (see Fig. S3 (d)), the stoichiometry of the SrZrO_3 buffer layer deteriorates at very high growth temperatures (above 1300°C) due to the volatility of SrO .

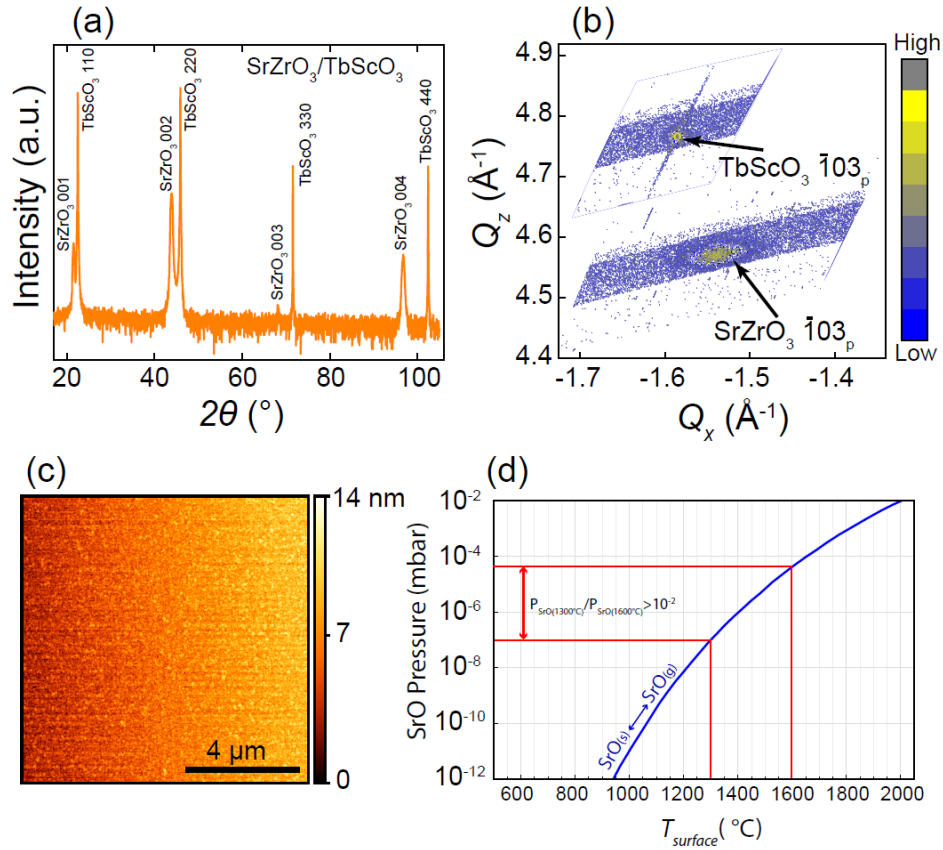


Figure S3: Characterization of the SrZrO_3 buffer layer. (a) $2\theta - \omega$ scan over a wider region for a 100 nm thick SrZrO_3 buffer layer grown at 1300 $^\circ\text{C}$ on a TbScO_3 substrate. Only the phase-pure $00l$ peaks from the SrZrO_3 film are observed. (b) Reciprocal space map and (c) AFM image of the same SrZrO_3 film. (d) SrO phase diagram (adapted from Ref.³).

TABLE S1. Overview of the extracted transport characteristics (mobility and carrier density) and lattice parameters for different $\text{La}:\text{BaSnO}_3$ (25 nm)/ SrZrO_3 (100 nm)/ TbScO_3 heterostructures for several growth temperatures of the SrZrO_3 buffer layer.

SrZrO ₃ growth temperature ($^\circ\text{C}$)	In-plane lattice constant	Out-of-plane lattice constant	Carrier density at 300 K (cm^{-3})	Mobility at 300 K ($\text{cm}^2 \text{V}^{-1} \text{s}^{-1}$)
	La:BaSnO ₃ a (\AA)	La:BaSnO ₃ c (\AA)		
850	4.09	4.136	1.8×10^{20}	50
1200	4.07	4.14	4.6×10^{20}	97.4
1300	4.103	4.113	5.2×10^{20}	140
1300	4.103	4.113	5.0×10^{20}	136.2
1400	4.10	4.115	4.7×10^{20}	127
1600	4.06	4.142	5×10^{20}	100.8

¹Wolfgang Braun, J. Cryst. Growth **477**, 50 (2017).

²Wolfgang Braun, J. Cryst. Growth **477**, 34 (2017).

³Roman Engel-Herbert, *Molecular beam epitaxy of complex oxides (Book chapter in Molecular Beam Epitaxy)*, edited by Mohamed Henini, Elsevier, Amsterdam, Pages: 417-449 (2013).